



HAL
open science

Semi-Lagrangian particle methods for high-dimensional Vlasov-Poisson systems

Georges-Henri Cottet

► **To cite this version:**

Georges-Henri Cottet. Semi-Lagrangian particle methods for high-dimensional Vlasov-Poisson systems. 2017. hal-01584107v2

HAL Id: hal-01584107

<https://hal.science/hal-01584107v2>

Preprint submitted on 18 Sep 2017 (v2), last revised 19 Apr 2018 (v3)

HAL is a multi-disciplinary open access archive for the deposit and dissemination of scientific research documents, whether they are published or not. The documents may come from teaching and research institutions in France or abroad, or from public or private research centers.

L'archive ouverte pluridisciplinaire **HAL**, est destinée au dépôt et à la diffusion de documents scientifiques de niveau recherche, publiés ou non, émanant des établissements d'enseignement et de recherche français ou étrangers, des laboratoires publics ou privés.

26 One drawback of particle methods is the inherent noise that affects their accuracy. This noise
27 results from the chaotic behavior of particles and makes it in general necessary to average particle
28 quantities on a large number of particles, which has a strong impact on their computational cost.

29 On the other hand, the advent of large supercomputers and parallel algorithms has made possible
30 the use of Eulerian methods to discretize the Vlasov-Poisson equation with a better accuracy. Two
31 important developments in this field have in particular been made in the recent years : semi-Lagrangian
32 and multi-resolution methods.

33 Semi-Lagrangian methods [19] are grid-based methods well adapted to the fact that the Vlasov
34 equation are advection-driven. At each grid point, particle trajectories are traced back in the phase
35 space and values on the solution are updated by interpolating the values of the distribution function at
36 the foot of the trajectory. Recent developments include the derivation of high order [5] and conservative
37 [6] methods. One drawback of the method still lies on its computational complexity, and its use, to
38 our knowledge, has so far been limited to low dimensional or small time simulations.

39 Multi-resolution methods are a rather attractive approach to address the dimension issue of Vlasov-
40 Poisson systems due to the ability of these methods to concentrate their effort on limited areas of the
41 computational domain. In [11] AMR techniques were devised and applied to two-dimensional problems.
42 Very recently, in [7] a wavelet-based approach was developed for the Vlasov-Poisson equations and
43 applied with success to 4 and 6 dimensional systems. The latter method gives rigorous and flexible
44 criteria to define the multi-resolution hierarchy grids. All these methods are however based on Eulerian
45 discretizations and they do not have the attractive robustness that Lagrangian or semi-Lagrangian
46 methods offer for the underlying transport equations. Note that multi-resolution semi-Lagrangian
47 methods have also been devised in the context of discontinuous Galerkin methods for the Vlasov
48 Poisson equations in [3] but their application has been so far restricted to 2D problems.

49 Going back to particle methods, recent development in the fields of transport equations and compu-
50 tational fluid dynamics have been made to overcome the accuracy limitations of these methods. Particle
51 remeshing on a regular grid, in particular, has been found to be an efficient way to avoid numerical
52 noise in flows submitted to high shear [13], while essentially preserving the localization properties
53 of particle methods. Remeshing particles at each time-step yields a class of forward, conservative,
54 semi-Lagrangian methods which can be analyzed as such [4]. The accuracy of these methods can be
55 analyzed in terms of the moment and regularity properties of the remeshing kernel. The localization

56 properties of semi-Lagrangian particle methods can be reinforced by using Adaptive Mesh Refinement
57 [1] or wavelet-based multi-resolution [2, 17]. To our knowledge, remeshed particle methods have not
58 been applied to the Vlasov-Poisson equations, with the notable exception of [15]. In this reference
59 the method is applied with success to the two-dimensional Vlasov-Poisson system (one space and one
60 velocity dimensions). The influence of the remeshing kernel in the overall accuracy of the method for
61 the Landau damping is discussed. The purpose of the present work is to investigate the capabilities of
62 semi-Lagrangian particle methods, both in terms of accuracy and computational complexity, to handle
63 4D and 6D Vlasov systems. The challenge is to determine splitting and remeshing strategies which are
64 tractable in high dimensions. To investigate these strategies we will restrict ourselves to single core
65 implementations of the method using an underlying uniform grid to remesh particles and we will use
66 the same benchmarks as in [7].

67 The outline of the paper is as follows. In section 2 we recall our previous work on semi-Lagrangian
68 particle methods. In section 3 we define our splitting and remeshing strategy in the case of multi-
69 dimensional Vlasov-Poisson system. In section 4 we discuss the application of the method on our
70 benchmarks. Section 5 is devoted to concluding remarks and indication of future works.

71 2. Semi-Lagrangian particle methods for transport equations

72 As we will see in the next sections, an efficient implementation of semi-Lagrangian particle methods
73 is based on a directional splitting where particles are successively pushed and remeshed along the
74 directions of the phase space. We can thus focus on the one-dimensional transport equation to describe
75 the method and discuss its convergence properties.

Let us consider the following 1D model linear advection problem for the unknown function f :

$$f_t + (af)_x = 0, x \in \mathbf{R}, t > 0, \quad (1)$$

where a is a given smooth velocity field. A particle method where particles are remeshed at each time
step can be recast as

$$f_i^{n+1} = \sum f_j^n \Gamma \left(\frac{x_j^{n+1} - x_i}{\Delta x} \right), i \in \mathbf{Z}^d, n \geq 0. \quad (2)$$

76 In the above equation Δx is the grid size on which particles are remeshed (assuming a regular grid),
77 x_j are the grid points and Γ is the remeshing interpolating kernel. x_j^{n+1} is the result of the advection
78 at time t_{n+1} of the particle located at x_j at time t_n .

To satisfy the conservation of successive moments of the distribution f , starting with the conservation of mass, the remeshing kernel Γ must satisfy moment properties that can be written as

$$\sum_{k \in \mathbf{Z}} (x - k)^\alpha \Gamma(x - k) = \begin{cases} 1 & \text{if } \alpha = 0 \\ 0 & \text{if } 1 \leq \alpha \leq p \end{cases}, \quad x \in \mathbf{R}, \quad (3)$$

for a given value of $p \geq 1$. An additional requirement is that Γ is globally in $W^{r+1, \infty}$ (which means that all his derivatives up to order $r + 1$ are bounded), is infinitely differentiable in each integer interval (in practice Γ is a polynomial in these intervals), and satisfies the interpolation property : $\Gamma(i - j) = \delta_{ij}$. In the simple case of an Euler explicit scheme to advect particles, $x_j^{n+1} = x_j + a(x_j, t_n)$ and when the time step satisfies the condition

$$\Delta t < |a'|_{L^\infty}^{-1}, \quad (4)$$

79 on can prove [4] that the consistency error of the semi-Lagrangian method is bounded by $O(\Delta t + \Delta x^\beta)$
80 where $\beta = \min(p, r)$. Using higher order Runge-Kutta schemes increase the time accuracy, as expected.
81 Moreover, at least for kernels of order up to 4, under appropriate decay properties for the kernel Γ one
82 can prove the stability of the method under the sole assumption (4).

83 A particular case, which will apply in the specific case of Vlasov-Poisson equations, where 'super
84 convergence' can be observed, is when, after an advection stage, each cell of size Δx contains exactly 1
85 particle (in other words when particle distortion along the line is limited). In that case the regularity
86 of the kernel 'across cells' is no longer necessary and the order of convergence β above is p instead of
87 $\min(p, r)$.

Kernels corresponding to specific values of p and r as described above are denoted by $\Lambda_{p,r}$. The following formulas give the expression of the kernels $\Lambda_{4,2}$ and $\Lambda_{8,4}$ which will be used in the sequel:

$$\Lambda_{4,2}(x) = \begin{cases} 1 - \frac{5}{4}|x|^2 - \frac{35}{12}|x|^3 + \frac{21}{4}|x|^4 - \frac{25}{12}|x|^5 & 0 \leq |x| < 1 \\ -4 + \frac{75}{4}|x| - \frac{245}{8}|x|^2 + \frac{545}{24}|x|^3 - \frac{63}{8}|x|^4 + \frac{25}{24}|x|^5 & 1 \leq |x| < 2 \\ 18 - \frac{153}{4}|x| + \frac{255}{8}|x|^2 - \frac{313}{24}|x|^3 + \frac{21}{8}|x|^4 - \frac{5}{24}|x|^5 & 2 \leq |x| < 3 \\ 0 & 3 \leq |x|, \end{cases} \quad (5)$$

$$\Lambda_{8,4}(x) = \begin{cases} 1 - \frac{205}{144}x^2 + \frac{91}{192}x^4 - \frac{6181}{320}x^5 + \frac{6337}{96}x^6 - \frac{2745}{32}x^7 + \frac{28909}{576}x^8 - \frac{3569}{320}x^9 & 0 \leq |x| < 1 \\ -154 + \frac{12757}{12}x - \frac{230123}{72}x^2 + \frac{264481}{48}x^3 - \frac{576499}{96}x^4 + \frac{686147}{160}x^5 & \\ \quad - \frac{96277}{48}x^6 + \frac{14221}{24}x^7 - \frac{28909}{288}x^8 + \frac{3569}{480}x^9 & 1 \leq |x| < 2 \\ \frac{68776}{7} - \frac{1038011}{28}x + \frac{31157515}{504}x^2 - \frac{956669}{16}x^3 + \frac{3548009}{96}x^4 - \frac{2422263}{160}x^5 & \\ \quad + \frac{197255}{48}x^6 - \frac{19959}{28}x^7 + \frac{144545}{2016}x^8 - \frac{3569}{1120}x^9 & 2 \leq |x| < 3 \\ -56375 + \frac{8314091}{56}x - \frac{49901303}{288}x^2 + \frac{3763529}{32}x^3 - \frac{19648027}{384}x^4 + \frac{9469163}{640}x^5 & \\ \quad - \frac{545977}{192}x^6 + \frac{156927}{448}x^7 - \frac{28909}{1152}x^8 + \frac{3569}{4480}x^9 & 3 \leq |x| < 4 \\ \frac{439375}{7} - \frac{64188125}{504}x + \frac{231125375}{2016}x^2 - \frac{17306975}{288}x^3 + \frac{7761805}{384}x^4 - \frac{2895587}{640}x^5 & \\ \quad + \frac{129391}{192}x^6 - \frac{259715}{4032}x^7 + \frac{28909}{8064}x^8 - \frac{3569}{40320}x^9 & 4 \leq |x| < 5 \\ 0 & 5 \leq |x|. \end{cases} \quad (6)$$

88 The kernel $\Lambda_{4,2}$ (resp $\Lambda_{8,4}$) involves a stencil made of 6 grid points (resp 10 grid points). The benefit
89 of using directional splitting is not only to reduce the analysis to the 1D case but also to minimize
90 the cost when high order kernels, with large stencils, are used. For instance, if a first order splitting is
91 used in 3 dimensions, the cost of the method for N particles with the $\Lambda_{4,2}$ (resp $\Lambda_{8,4}$) kernels will scale
92 as $O(18N)$ (resp $O(30N)$) instead of $O(216N)$ (resp $O(1000N)$) if a tensor product formula was used.

93 3. Algorithm for the Vlasov-Poisson equations

94 As already mentioned, remeshed particle methods have already been applied to 1D/1D Vlasov
95 Poisson system in [15]. In this reference, the gain offered by fourth order methods has been demon-
96 strated on the analysis of the one-dimensional Landau damping. In this section and the following we
97 present an implementation of semi-Lagrangian particle methods for the 6D Vlasov-Poisson system,
98 where we in particular emphasize the role of directional splitting and link-list algorithms to reduce the
99 computational complexity and we further investigate the influence of high order kernels to improve the
100 accuracy of the methods. We denote by x, y, z and u, v, w the space and velocity axis, respectively.

101 Particle remeshing which is essential for accuracy control also results in the need to introduce
102 grid arrays. On the one hand, using six dimensional arrays is not affordable, except for very coarse
103 resolutions. On the other hand using directional splitting, as suggested in the previous section, would
104 in principle only require one-dimensional arrays to carry particle quantities but each line would have
105 to be labelled with a five-dimensional array, which is also intractable.

106 A reasonable trade-off between splitting and array dimensions is to alternate motion/remeshing of
107 particles in three dimensional spaces. The natural choice is to move/remesh particles in x, y, z and

108 u, v, w spaces alternately.

109 In the sequel, at the end of each remeshing step and for each (x, y, z) or (u, v, w) grid values, we
110 will call (x, y, z) -space (resp. (u, v, w) -space) a 3D array of particles with given x, y, z locations (resp.
111 (u, v, w) velocities) on the grid. To identify particles in such paces, a link-list algorithm is used. Link
112 list algorithms have long been used in grid-free particle methods, either to compute velocities in tree
113 codes or to compute diffusion through Particle Strength Exchange algorithms. In the present case, the
114 computation of densities can be made inside the link list algorithm used to label (x, y, z) -spaces by
115 accumulating values of f at a given (x, y, z) -location while sweeping over all particles. The results of
116 each of these link-list algorithms are (for the x, y, z linklist to fix ideas) :

- 117 • two three-dimensional arrays : a pointer which goes from the grid values to the index of the
118 particle, and the number of particles in each (x, y, z) -space,
- 119 • two arrays with dimension the total number of particles to specify indices of particles of the
120 planes in the original list of particles.

121 Once particles are assigned in given three-dimensional spaces, they can be advected along the corre-
122 sponding directions.

123 Assuming a first order time-splitting, the algorithm thus goes along the following steps, for each time-
124 iteration :

- 125 1. create link-list for (u, v, w) -spaces
- 126 2. in each (u, v, w) -space push particles in the x, y, z directions using the allocated u, v, w values
- 127 3. remesh particles and create fresh particles whenever the value of f exceeds a given threshold
- 128 4. create link-list for (x, y, z) -spaces and compute the density values
- 129 5. collect all densities and compute the electric field through a 3D Poisson solver
- 130 6. in each (x, y, z) -space push particles in the u, v, w directions using the electric field at the corre-
131 sponding x, y, z location.
- 132 7. remesh particles and create fresh particles whenever the value of f exceeds a given threshold.

133 In the sequel we use a second order time-splitting method, where the step 1 to 3 above are made over
134 half a time-step and repeated at the end of the iteration.

135 As mentioned in section 2, using high order remeshing kernels can lead to high computational cost
136 if a 3D tensor-product remeshing formula is used. For this reason, steps 2-3 and 6-7 above are in turn
137 split into one-dimensional advection-remeshing steps. To do so, one could again use link-list algorithms
138 inside each three dimensional space to assign particles to lines. An alternative, more direct, solution is
139 to successively advect the three-dimensional spaces by freezing 2 out of the 3 indices. Note that when
140 using this additional splitting in, say, a given (x, y, z) -space, the link-lists are used only in the first
141 direction. After advection-remeshing along the first direction, arrays of particles are created in the
142 given (x, y, z) -space and used, instead of the link-lists, in the subsequent stages of the splitting in that
143 specific space. As a result, advection/remeshing in the 2 subsequent directions of the (x, y, z) -space
144 are faster (typically by a factor 2 in our implementation).

145 A few remarks on the cost and accuracy of this algorithm are now in order.

146 From the computational point of view, at the end of the remeshing steps when new particle values
147 are assigned from the grid values, in order to limit the cost of this step to the number of particles
148 and not to 6-dimensional full grids, it is important to avoid sweeping over the whole three-dimensional
149 spaces. To do so, nearest grid points assigned to particles after particle motion are identified in stages
150 2 and 6 above, and when one has to assign grid values to fresh particles, one only considers these grid
151 points and neighboring grid points (the number of which depends on the size of the support of the
152 remeshing kernel).

153 From the accuracy point of view, one can make the following important observations :

154 1) In each (u, v, w) -space the velocity in the (x, y, z) directions is constant. Therefore pushing particles
155 with a simple first-order Euler scheme gives exact solution of the particle advection (and similarly in
156 the (x, y, z) -spaces). In other words, the time accuracy of the overall scheme is only dictated by the
157 Ξ/Ψ splitting algorithm.

158 2) For the same reason, one-dimensional splitting within each 3D space does not introduce further
159 splitting error.

160 3) In section 2 above we have indicated that the regularity of the kernels is a limiting factor in the
161 overall accuracy of the method, except when the advection of particles maintains exactly one particle
162 in each grid cell. We are precisely in this particular case, since, for each splitting sub-step, on each
163 line particles are advected by a constant velocity. In other words advection-remeshing with the kernel
164 $\Lambda_{2,1}$ is second order, fourth order with $\Lambda_{4,2}$, and so on.

165 4) For the same reason, the Lagrangian CFL condition (4) does not give in the present implementation
166 any limitation for the time-step.

167 5) Finally, we recall that remeshing kernels which provide second order approximations, or beyond, are
168 not positive. In the steps 3 and 7 above, one can apply the threshold either on the absolute value of f ,
169 in which case negative values of f can appear, or to the value of f itself, which ensures the positivity
170 of f but may compromise the conservativity of the algorithm. We will comment on this specific aspect
171 in the sequel.

172 The stability property just mentioned in 4) is in principle desirable, since it ensures unconditional
173 stability of the method. However it has the drawback of not giving a clear criterion to choose the
174 time-step, in contrast with semi-Lagrangian particle methods for flow simulations where the time-step
175 is in general defined as a function of the maximum amount of shear in the flow. One way to determine
176 the time-step value would be to control the accuracy of the Ξ/Ψ splitting, which, as we have already
177 noticed, controls the overall time-accuracy of the method. One can easily check that the accuracy of
178 this splitting is given by the spatial derivatives of the velocity field in the phase space. In the particular
179 case of the Vlasov-Poisson equations, these derivatives reduce to 1, on the one hand, and the spatial
180 derivatives of the electric field on the other hand. Derivatives of the electric field are in turn bounded in
181 terms of the density. As a result, one quantity to monitor and that can be used to adapt the time-step
182 value is the maximum value of the density. In practice we have chosen fixed time-step values which
183 were a fraction of the maximum density. As we will see, for the grid-size used in our simulations these
184 values eventually correspond to large CFL numbers.

185 Let us finally comment on the memory foot-print and computational complexity of the method.
186 The memory load is directly given by the number of particles. More precisely, for a six-dimensional
187 phase space the algorithm outlined above requires in our implementation 16 arrays of size the number
188 of particles:

- 189 • 7 main arrays, for the 3 axis and velocity directions and for the distribution function,
- 190 • 7 additional arrays which are used to temporary store particle locations and velocities during the
191 push and remesh algorithms,
- 192 • 2 arrays to store particles addresses computed in the link list algorithms and used to push and
193 remesh particles in the 3D spaces.

194 On top of these particles arrays, the algorithm requires several 3D arrays, but with a memory size
 195 which is a small fraction of that of the particle arrays. In most of our simulations the number of
 196 particles was of the order of 10^8 for a number of grid points in each 3D space of the order of 10^6 . In
 197 the next section we will show the computational time involved at each stage of the algorithm.

198 4. Four and Six dimensional benchmarks

199 In this section we focus on two cases borrowed from [7] and which illustrates the capabilities and
 200 limits of the method in single core implementations : a 4D plasma instability and a 6D gravitational
 201 case. All our simulations were performed on an Intel Xeon E5-2640 core running at 2.5GHz.

202 4.1. Four dimensional two-beams instability

In this section we consider the Fijalkow Two Beams instability [9]. Following [7] the initial condition is given by the following formula

$$f_0(x, y, u, v) = \frac{7}{4\pi} \exp\left(-\frac{u^2 + 4v^2}{8}\right) \sin^2\left(\frac{u}{3}\right) (1 + 0.05 \cos(0.3x)), \quad (7)$$

and the computational box is the the rectangle

$$\Omega = \left[-\frac{10\pi}{3}, \frac{10\pi}{3}\right] \times [-3\pi, 3\pi].$$

203 For this case, we used the remeshing kernel $\Lambda_{4,2}$ given by (5), which conserves the four first moments
 204 of the distribution function (and, as a result, is not positive) and which is twice differentiable. We
 205 recall that, although in principle this remeshing kernel leads to a second order transport scheme, in the
 206 particular case of the Vlasov Poisson equation with directional splitting it yields fourth order spatial
 207 accuracy.

208 The cut-off value to create particles at the end of the remeshing step was taken equal to 10^{-5} and it
 209 was applied to the value of f and not its absolute values. In particular this has the effect of discarding
 210 any negative values which could result from the remeshing kernel.

211 In the first experiment we monitor the conservation properties of the method and we use two sets
 212 of resolutions : a coarse grid with $N_c = 64^4$ grid points and a finer grid using $N_f = 128^4$ grid points.
 213 We compare our results to the wavelet-based multi-resolution Eulerian solver in [7], with equivalent
 214 grid-sizes ranging from 32^4 , at the coarsest level, to 256^4 at the finest level, and which is based on a
 215 third order finite-difference scheme.

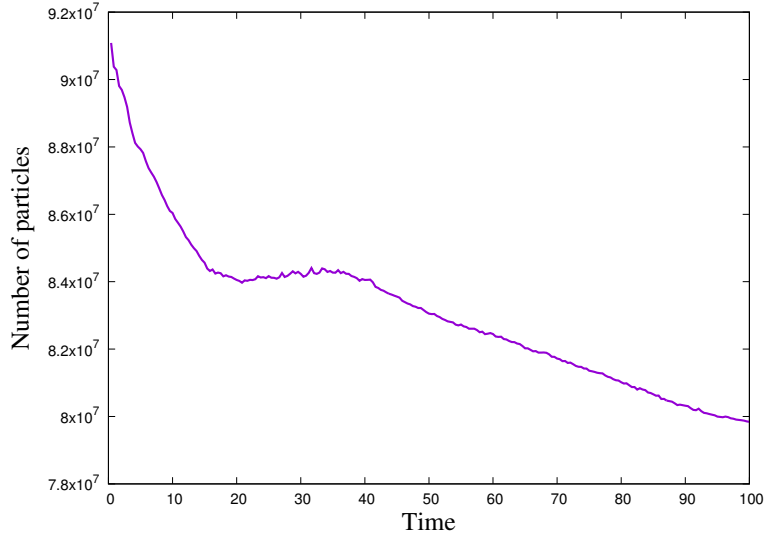


Figure 1: Number of particles for the 4D Vlasov-Poisson two-beams instability with initial condition (7) and 128^4 effective grid resolution.

216 As already mentioned, in the particular case of the Vlasov-Poisson equation, the semi-Lagrangian
 217 particle method is unconditionally stable, and the time accuracy of the algorithm is only dictated by
 218 the $(x, y, z)/(u, v, w)$ splitting. This splitting error is governed by the derivatives of velocity in the
 219 phase space, which are equal to 1 (for the three first components) and the spatial derivative of the
 220 electric field. For periodic boundary conditions, in energy norms these derivatives are in turn bounded
 221 by the density. In all our experiments the density value did not exceed 1 and we chose a constant
 222 value of 0.4 for the time-step. This time-step value correspond to a CFL value, based on the maximum
 223 particle velocity in the box, of 9 in the coarse grid case, and 18 in the finer grid case. Taking smaller
 224 time steps did not change the results shown below.

225 Unlike in mesh-free particle methods, in semi-Lagrangian particle methods the support of the
 226 density function can increase as a result of remeshing. To measure this spreading effect we show in
 227 Figure 1 the particle numbers as a function of time for our run using the 128^4 grid. Surprisingly, the
 228 number of particles slightly decrease to settle to a value around $8 \cdot 10^7$. For comparison, the multi-
 229 resolution method of [7] with equivalent resolution between 32^4 and 256^4 , used, beyond time $t = 10$,
 230 between $5 \cdot 10^6$ and $6 \cdot 10^7$ active grid points.

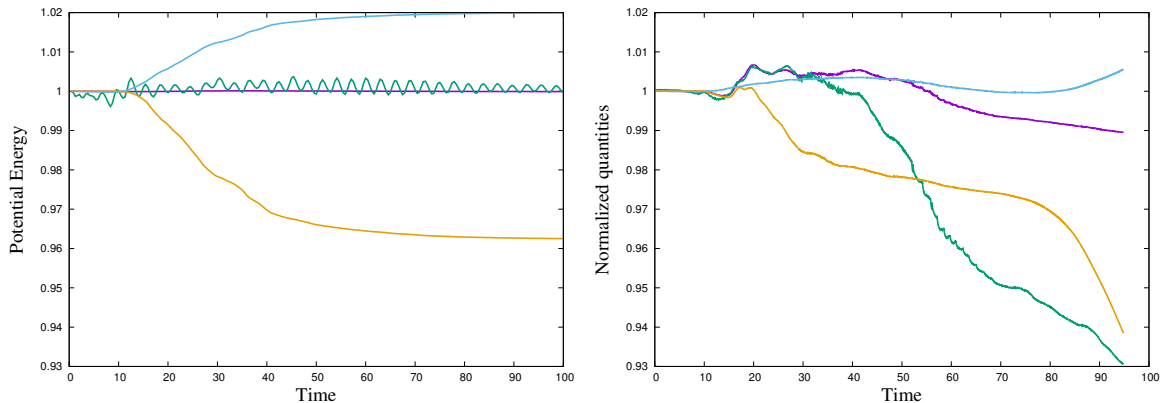


Figure 2: Conservation properties for the same case as in Fig 1. Left picture : present method; right picture : multi-resolution method of [7]. Magenta curve : mass; green curve : total energy; yellow curve : norm L^2 of f ; bleu curve : entropy.

231 We now turn to the conservation properties of the method. Figure 2 shows total mass, energy,
 232 entropy and L^2 norm of the distribution function f , normalized by their initial value, compared to the
 233 same quantities as obtained in [7]. Some observations can be made from these graphs, which highlight
 234 the differences between semi-Lagrangian schemes and Eulerian schemes. The conservation of mass and
 235 energy is almost perfect in the particle method, whereas in the calculations of [7] the energy tends
 236 to dissipate. The conservation of mass indicates that negative values resulting from remeshing with a
 237 fourth order kernel, and which in our implementation are discarded after remeshing, would only have
 238 marginal contributions. This confirms a similar observation made in [15]. The L^2 norm of f drops at
 239 about 96% of its initial value then settles. The entropy increases by 2% then settles.

240 A further comparison of the solutions given by the two methods is given by Figure 3. This figure
 241 shows cuts of the distribution function in the (x, u) plane, at $y = v = 0$ at time $t = 12$, when the
 242 potential energy reaches its peak value (see Figure 6 for the time history of the potential energy). The
 243 two results are in perfect agreement.

244 We now show the results obtained with a coarser background grid using 64^4 points and the same
 245 time step value $\Delta t = 0.4$. Figure 4 shows the conservation properties for this coarse grid compared to
 246 the finer grid. One can see that even for the coarse grid the method conserves pretty well the invariants
 247 of the Vlasov-Poisson system. The good performance of the coarse grid simulation is confirmed by a

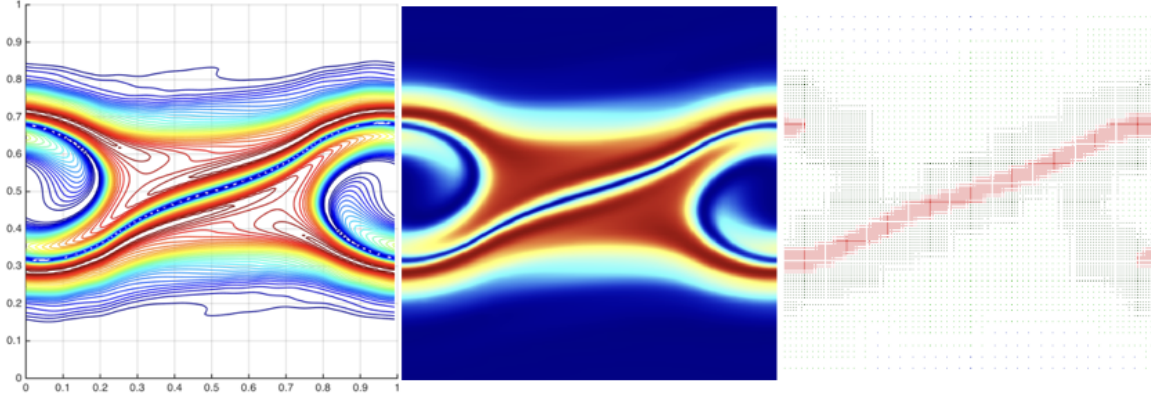


Figure 3: Same case as in Fig 1. Cut of the distribution function in the plane (x, u) at $y = v = 0$ and $t = 12$. Left picture : present method; middle picture : result of [7]; right picture : multi-resolution grid used in [7] (red zones correspond to an equivalent resolution of 256 grid points).

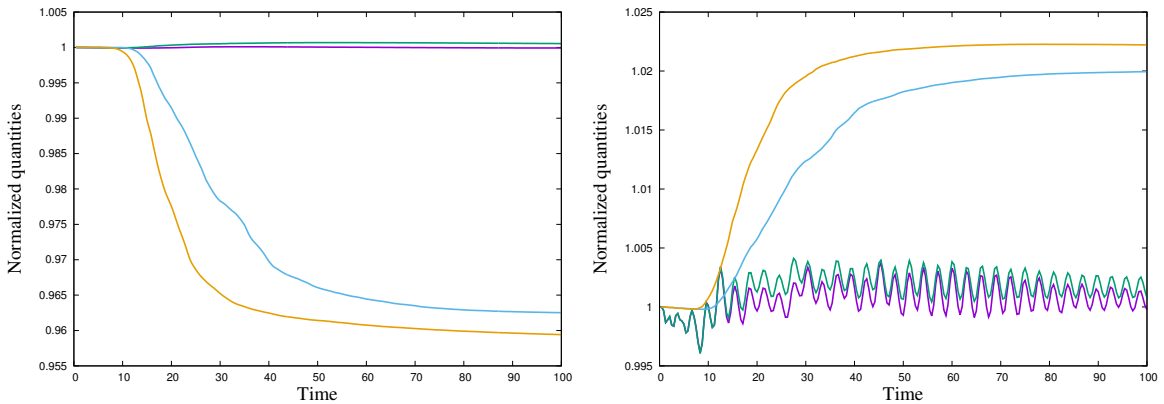


Figure 4: Vlasov-Poisson two-beams instability with initial condition (7). Conservation properties with the present method based on coarse grid (CG, 64^4) and fine grid (FG, 128^4) grids. Left picture : mass (magenta curve : FG, green curve : CG); norm L^2 of f (blue curve : FG, yellow curve : CG). Right picture : energy (magenta curve : FG, green curve : CG); entropy (blue curve : FG, yellow curve : CG).

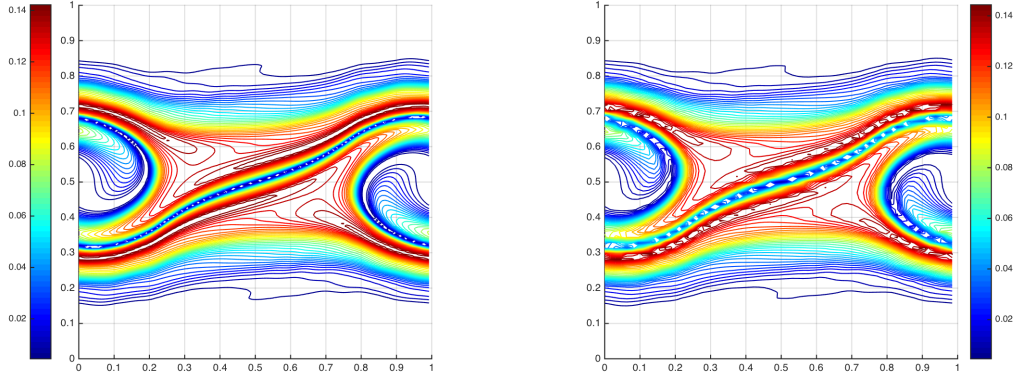


Figure 5: Vlasov-Poisson two-beams instability with initial condition (7). Cut in the plane (x, u) at $y = v = 0$ of the distribution function f with the present method based on coarse grid (CG, 64^4) and fine grid (FG, 128^4) grids. Left picture : FG; right picture : CG.

248 comparison of the cross section of f in the (x, u) plane at time $t = 12$ (figure 5). A more challenging
 249 comparison between the two resolutions can be made by looking at the potential energy $1/2 \int E^2$
 250 alone (Figure 6). One can see that the two resolutions give the same profile during the instability
 251 growth and oscillate around the same level for later times. The results of [7] by contrast show that the
 252 inherent dissipation in the underlying finite-difference scheme does not allow to maintain the potential
 253 energy at its correct level. These comparisons allow to conclude that the semi-Lagrangian particle
 254 method retains the desirable conservation properties of grid-free particle methods and gives rather well
 255 converged results even at coarse resolutions.

256 The CPU time required to perform the computation up to time $t = 100$ for the 128^4 resolution, with
 257 a particle number around $8 \cdot 10^7$ particles, was about 5.5 hours, for 250 iterations. The breakdown of the
 258 computational cost between the link-list operations on the one hand and the particle-grid interpolations
 259 and particle assignment involved in the remeshing stages on the other hand, is given in Figure 7. The
 260 other parts of the algorithms, including the FFT-based field evaluations, are responsible for less than
 261 1% of the computational cost and are not shown on this graph. The memory size required for the
 262 higher resolution run was 7Go.

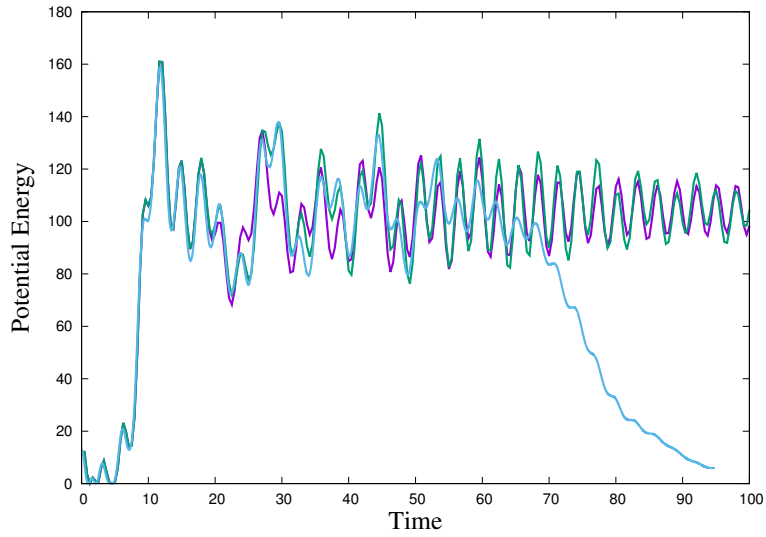


Figure 6: Vlasov-Poisson two-beams instability with initial condition (7). Potential energy obtained with the present method with a 128^4 grid (green curve) and with a 64^4 grid (magenta curve) compared to the method in [7] (blue curve).

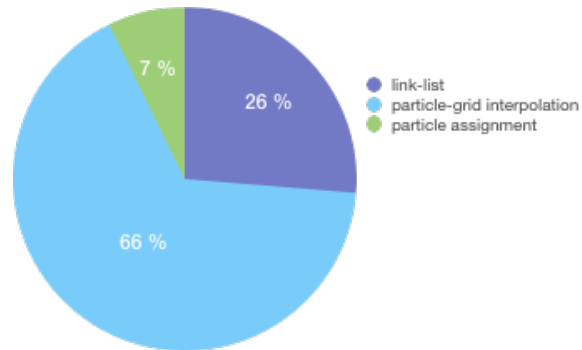


Figure 7: Breakdown of computational cost in the semi-Lagrangian particle method for the two-beams Vlasov-Poisson instability.

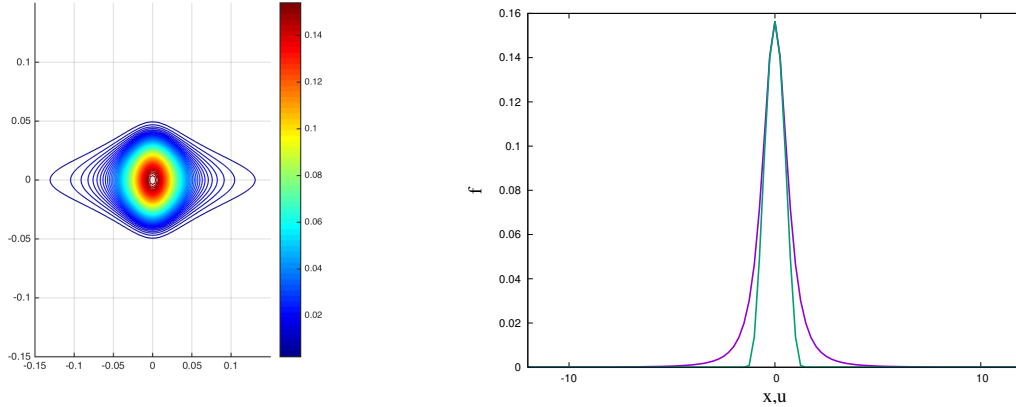


Figure 8: Cross section in the plane (x, u) (left picture) and 1D cuts (right picture) corresponding to the distribution function given by (8). Green (resp magenta) curve : cut in the u (resp x) direction.

263 4.2. Six dimensional gravitational case

264 We now turn to a more challenging case which involves a six-dimensional Vlasov-Poisson system.
 265 We consider the case of two density blobs, each determined by a steady-state Plummer model [10],
 266 and interacting with each other. Again we will compare our results with the multi-resolution results
 267 of [7], using equivalent resolutions ranging between 32^6 and 512^6 , and also with results shown in this
 268 reference and provided by the GADGET grid-free particle software [20] (see Table 1 for the parameters
 269 of these simulations).

The distribution function of each blob is given by the following formula :

$$f_p(\Xi, \Psi) = \begin{cases} \frac{3}{7\pi^3} (2(1 + |\Xi|^2)^{-1/2} - |\Psi|^2)^{7/2}, & \text{if } 2(1 + |\Xi|^2)^{-1/2} - |\Psi|^2 \geq 0 \\ 0 & \text{otherwise,} \end{cases} \quad (8)$$

270 where $\Xi = (x, y, z)$ and $\Psi = (u, v, w)$ (see Figure 8). This distribution function leads to a steady-state
 271 solution of the Vlasov Poisson system with unit density. Figure 8 shows 2D and 1D cuts of f in the
 272 (x, u) plane, with all other variables set to 0.

Following [7] we choose an initial condition given by

$$f_0(x, y, z, u, v, w) = f_p(x - a_0, y, z - b_0, u - c_0, v, w) + f_p(x, y - a_0, z + b_0, u, v - c_0, w), \quad (9)$$

with $a_0 = -6$, $b_0 = -2$, $c_0 = 0.3$, in the box $\Omega = [-12, +12]^6$. The Poisson equation to obtain the

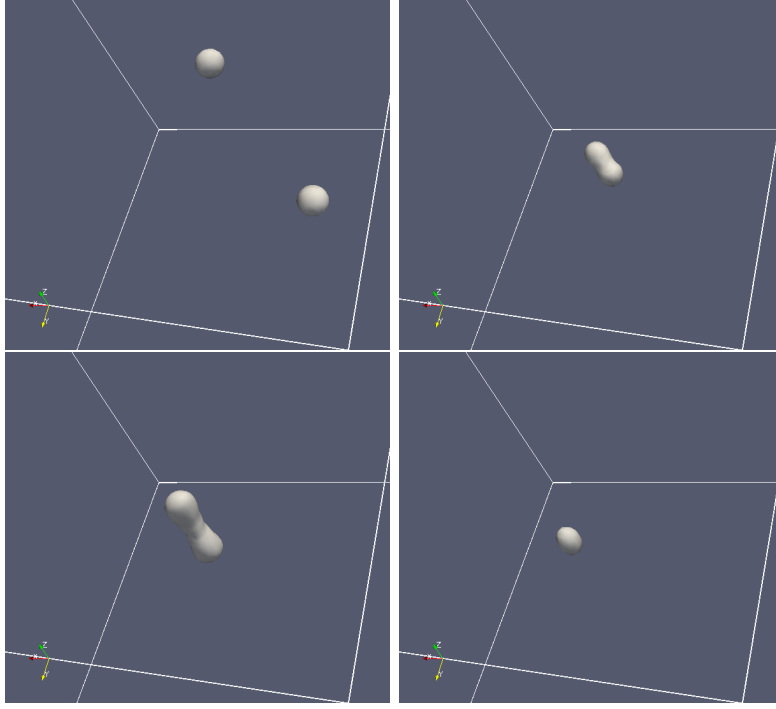


Figure 9: Density rendering for the initial condition (9) at times (from left to right, top to bottom) 0.7, 15.4, 20 and 25.6. Isosurfaces correspond to one third of the maximum density which is respectively 0.22, 0.36, 0.11 and 0.35.

gravity field $E = -\nabla\Phi$ from the density $\rho(\Xi) = \int f(\Xi, \Psi) d\Psi$ is

$$\Delta\phi = 4\pi(\rho - \bar{\rho}),$$

273 where $\bar{\rho} = 1/|\Omega| \int \rho d\Xi d\Psi$, with periodic boundary conditions The interaction of the two blobs produce
 274 a complex dynamics as they collide then separate then collide again, as shown in Figure 9.

275 This case is more challenging than the previous one not only because of the dimension of the phase
 276 space but also because of the sharp profile of the distribution function. For high order finite-difference
 277 and semi-Lagrangian particle methods as well, this means that negative values and spurious oscillations
 278 are expected to arise.

279 As a matter of fact, and in strong contrast with the previous case, it turns out that discarding
 280 negative values in the remeshing stages of our algorithm as described in section 3 would severely
 281 damage the conservation of its invariants. A second observation is that, to obtain correct conservation

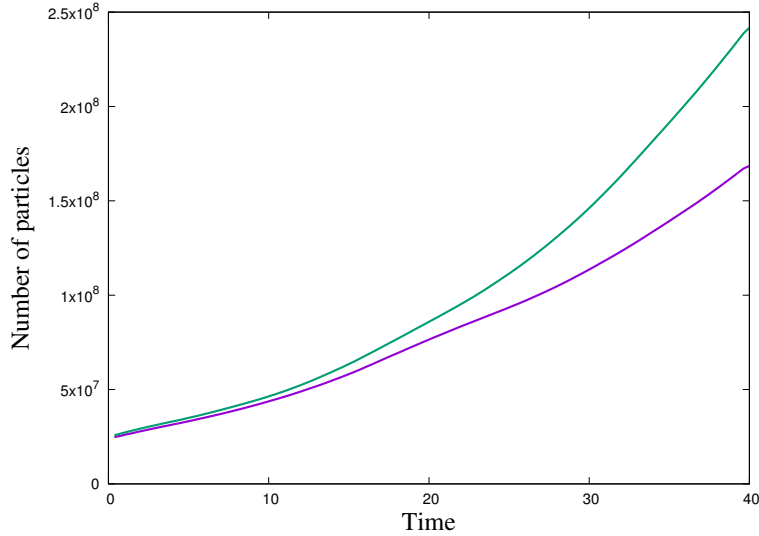


Figure 10: Number of particles for the initial condition (9) and an underlying grid of 96^6 points with 4th and 8th order methods. Magenta curve : kernel $\Lambda_{4,2}$; green curve : kernel $\Lambda_{8,4}$.

282 properties, we found it necessary to decrease the threshold value to 10^{-6} , and therefore increase the
 283 number of particles.

284 Like in the previous case, we set the time-step value to $\Delta t = 0.4$ for all our simulations. Figure 10
 285 shows the number of particles as time goes on with the semi-Lagrangian particle method using the
 286 kernel $\Lambda_{4,2}$ and an underlying grid of 96^6 points. In that case the CFL number corresponding to our
 287 time-step and the maximum velocity value on particles is around 6. For comparison, the multilevel
 288 method of [7] with equivalent resolutions between 32^6 and 512^6 used a maximum of about $5 \cdot 10^9$ grid
 289 points in the same time interval and a time step varying between $1.2 \cdot 10^{-2}$ and $3 \cdot 10^{-2}$. The increase in
 290 the number of particles, which contrasts with what was observed in the previous section, results from
 291 the need to resolve small scales produced by the dynamics but also spurious oscillations created by
 292 particle remeshing. This simulation used about 24 Go of RAM memory.

293 In Figure 11 we check the conservation of mass, entropy and L^2 norm of f compared to the multi-
 294 resolution method of [7]. One can see that, except for the total mass, the invariants produced by the
 295 particle method rapidly show some discrepancy, in particular for the L^2 norm of f . This is confirmed
 296 by the time history of the kinetic energy $E_k = 1/2 \int f(\Xi, \Psi) |\Psi|^2 d\Xi d\Psi$. Figure 12 shows how our

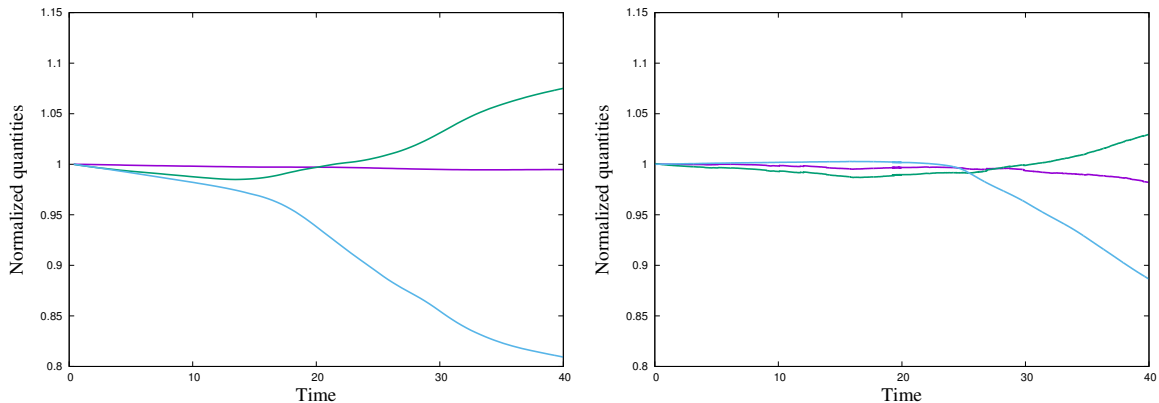


Figure 11: Conservation properties for the gravity test (9). Left picture : present method with kernel $\Lambda_{4,2}$ and 96^6 grid. Right picture : multi-resolution method [7]. Magenta curves: total mass; green curves : entropy; blue curves : norm L^2 . Quantities are normalized by their initial value.

297 method, with the 96^6 resolution and the kernel $\Lambda_{4,2}$ compares with the multi-resolution method of [7]
 298 and also with the result of the GADGET software using $5 \cdot 10^8$ particles.

299 To investigate whether higher order particle methods could improve these diagnostics, we next
 300 tested the $\Lambda_{8,4}$ kernel given by formula (6). Figure 10 gives a comparison of the increase in number
 301 of particles which results from this remeshing formula with that obtained with the previous kernel.
 302 Figure 13 shows the selected invariants and the kinetic energy when this 8th order method is used.
 303 With this higher order kernel, the loss in the L^2 norm of f is significantly reduced, in particular in
 304 the early stage of the simulation, and the method gives an excellent fit with GADGET for the kinetic
 305 energy. Although with a much lower maximum resolution, it avoids at the late stage of the simulation
 306 the numerical dissipation of the underlying finite-difference method in the MRA method of [7]. Note
 307 that an implementation of the method of [7] with a finest level of refinement corresponding to a 256^6
 308 grid instead of 512^6 does not give the correct energy profile for the second collision around $t = 25$ [8].

309 The improvement provided by the high order kernel is even clearer on lower resolution simulations.
 310 Figure 14 shows the result obtained at a coarse resolution corresponding to a 64^6 grid. The high order
 311 kernel already provides reasonable results at this low resolution, albeit with a delayed second collision
 312 and at a lower level, whereas the 4th order kernel in particular totally fails to reproduce the second
 313 collision in the kinetic energy.

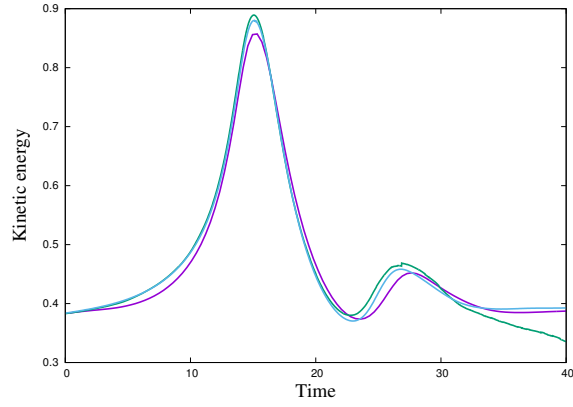


Figure 12: Kinetic energy for the gravity test (9). Magenta curve : present method with kernel $\Lambda_{4,2}$ and 96^6 grid; green curve : mutli-resolution method [7] ; blue curve : GADGET simulation [7].

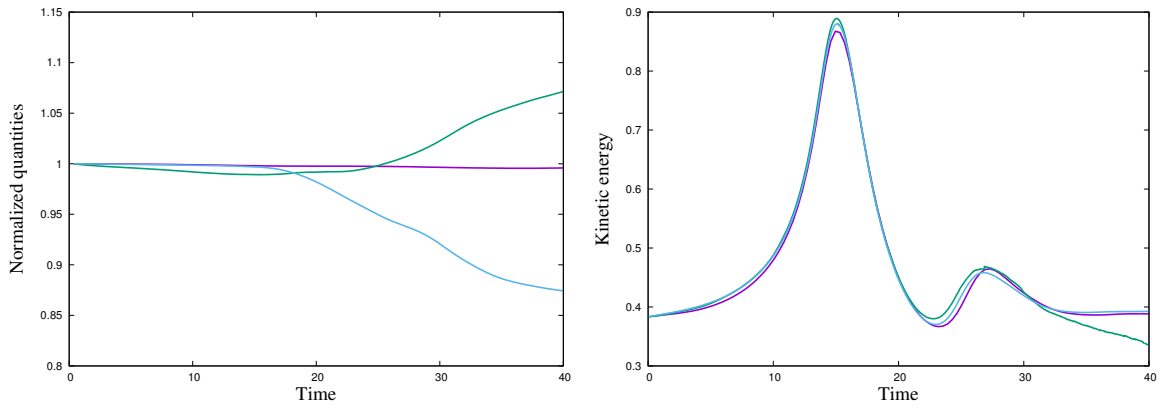


Figure 13: Left picture : same as Figure 11 with kernel $\Lambda_{8,4}$. Right picture : same as Figure 12 with kernel $\Lambda_{8,4}$.

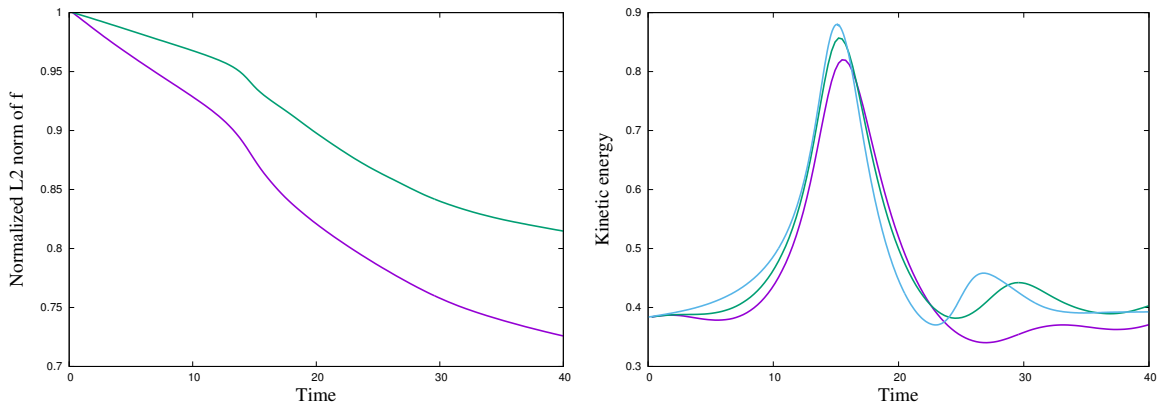


Figure 14: Comparison of the methods using $\Lambda_{4,2}$ (magenta curves) and $\Lambda_{8,4}$ (green curves) kernels on a 64^6 grid. Left picture : L^2 norm of f ; right picture : kinetic energy (blue curve is the reference GADGET result).

314 The satisfactory behavior of semi-Lagrangian particle methods to reproduce energy profiles and
 315 conserve invariants with affordable resolution should however not hide the fact that this resolution is not
 316 sufficient if one desires to obtain accurate local values of the distribution function. The comparison with
 317 the results obtained in multi-level method of [7] in Figure15 shows that the 96^6 equivalent resolution
 318 has difficulties to represent accurately the local values of the distribution function beyond time $t = 16$.
 319 Another caveat concerning the present method is that, as already mentioned, it does not preserve the
 320 positivity of the distribution function (note however that density values always remain positive). This
 321 difficulty, also present in the multi-resolution calculations in [7], is inherently linked to the use of high
 322 order (and thus non positive) interpolation kernel. It is possible to derive semi-Lagrangian methods
 323 with TVD limiters [14], but in the present case these methods proved to be over dissipative. Deriving
 324 along the same lines Weno type remeshing formulas is certainly possible but has not yet been tried. It
 325 could be fruitful in the present applications.

326 We now come to the computational complexity of the method. Table 1 compares the computational
 327 cost of the present method, with the two kernels used in our simulations, to those of the multi-resolution
 328 and GADGET simulations reported in [7].

329 One can first observe that the ratio in CPU times between semi-Lagrangian particle methods based
 330 on the $\Lambda_{4,2}$ and $\Lambda_{8,4}$ kernels matches pretty well the ratio between the size of their stencils (6 points vs
 331 10 points). This indirectly confirms that using 3D tensor product formulas instead of splitting based

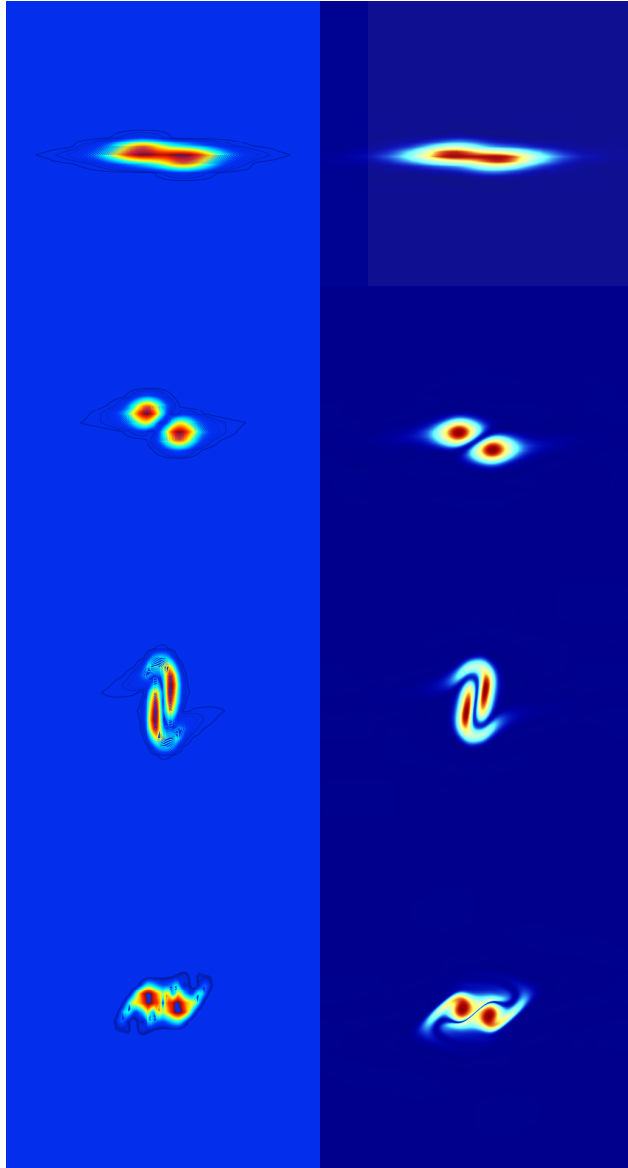


Figure 15: Cuts in the plane (z, w) for the gravity test. Left column : present method with 96^6 resolution and $\Lambda_{8,4}$ kernel; right column : [7]. From top to bottom, times are 6, 12, 16 and 20.

	4th order SL PM	8th order SL PM	Wavelet MRA [7]	GADGET [7]
Effective grid resolution	96	96	32 to 512	N.A.
Maximum number of active grid-points / particles	$1.8 \cdot 10^8$	$2.5 \cdot 10^8$	$5 \cdot 10^9$	$5 \cdot 10^8$
Number of time-steps	100	100	1349	N.A.
Wall clock CPU time	3.5 hours	5.8 hours	120 days	1 week
Hardware	1 Intel Xeon E5-2640 2.5 GHz	1 Intel Xeon E5-2640 2.5 GHz	32 Intel Xeon X5650 2.66GHz	500 cores

Table 1: CPU times for the present method, the multi-resolution method [7] and the GADGET software.

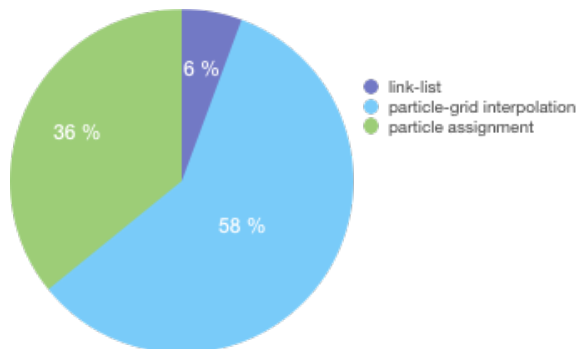


Figure 16: Computational cost of the various stages of the semi-Lagrangian method for the 6D gravitational test.

332 formulas would significantly increase the computational cost of these methods. As already noted, the
 333 large CPU time required in the GADGET simulation results from the need to consider blobs containing
 334 many particles in the field calculation. We believe that the significant speed-up provided by the particle
 335 method compared to the multi-resolution method in [7] is not only due to a larger time step and a
 336 smaller number of particles, but also to its algorithmic simplicity. It is actually interesting to note that,
 337 assuming enough memory to run the particle method on an underlying uniform 512^6 grid, which is the
 338 maximum resolution in [7], and a perfect scaling of the CPU time, since in the particle method the
 339 time-step is independent of the spatial resolution the 4th order method would require about 3350 days
 340 on a single core, which compares well with the 120 days on 32 cores in [7]. The main advantage of the
 341 multi-resolution approach seems to be in the memory requirement (the high resolution simulation in
 342 [7] *only* requires 512 Go while we already need 24 Go). One can conclude that the localization property
 343 of semi-Lagrangian particle methods combined with their accuracy and algorithmic simplicity make
 344 them suitable for large scale computations even when used with uniform grids.

345 The breakdown of the computational time in the main stages of the algorithm is given in Figure 16.
 346 It shows the same trends as in the previous 4D case, with however a reduced contribution of the link-list
 347 algorithm, due to the fact that this part of the method does not increase with the dimension of the
 348 problem, and an increased contribution of the assignment stages at the end of the remeshing steps.

349 5. Conclusion

350 In this paper we have presented implementations of high order semi-Lagrangian particle methods
351 that could handle high dimensional Vlasov-Poisson systems on uniform grids with attractive trade-off
352 between CPU costs and accuracy. The method was tested against state-of-the-art multi-resolution and
353 grid-free particle methods in a 4D plasma instability case and in a 6D gravitational case. In both
354 cases, the possibility to use large time-steps without compromising neither stability nor accuracy was
355 verified. In the first test, the method gives excellent results, even at coarse resolution, both in terms
356 of global quantities and local values. The 6D case shows the benefit of using high order kernels and
357 accurate global quantities are satisfactorily recovered at reasonable computational cost. The need of
358 multi-resolution is however apparent if accurate local values of the distribution function are sought in
359 long time simulations.

360 Future work will therefore be to implement a multi-resolution semi-Lagrangian particle method,
361 along the lines of [17]. Given the reduced CPU costs already observed for uniform grids, the goal
362 of multi-level particle methods will especially be to reduce the memory foot-print. The splitting
363 strategy implemented in the present work also lends itself to parallel implementations, including on
364 GPU processors [16, 4] or in hybrid GPU/CPU platforms [18], which gives another direction for future
365 research. One can expect from these further developments a valuable tool to address challenging
366 multi-dimensional plasma or gravitational systems.

367 Acknowledgements

368 The author is grateful to Erwan Deriaz for kindly sharing his data and for enlightening discussions
369 during the preparation of this work.

370 References

- 371 [1] M. Bergdorf, G.-H. Cottet and P. Koumoutsakos, Multilevel Adaptive Particle Methods for
372 Convection-Diffusion Equations, *SIAM Multiscale Modeling and Simulation* 4 (2005) 328–357.
- 373 [2] M. Bergdorf and P. Koumoutsakos, A Lagrangian Particle-Wavelet Method, *SIAM Multiscale*
374 *Modeling and Simulation* 5 (2006) 980–995.

- 375 [3] N.Besse, E. Deriaz and E. Madaule, Adaptive multiresolution semi-Lagrangian discontinuous
376 Galerkin methods for the Vlasov equations, *J. Comput. Phys.* 332 (2017) 376–417.
- 377 [4] G.-H. Cottet, J.-M. Etancelin, F. Perignon and C. Picard, High order Semi-Lagrangian particles
378 for transport equations: numerical analysis and implementation issues, *ESAIM: Mathematical*
379 *Modelling and Numerical Analysis* 48 (2014) 1029–1060.
- 380 [5] N. Crouseilles, T. Respaud and E. Sonnendrucker, A forward semi-Lagrangian method for the
381 numerical solution of the Vlasov equation, *Computer Physics Communications* 180 (2009) 1730–
382 1745.
- 383 [6] N. Crouseilles, M. Mehrenberger and E. Sonnendrucker, Conservative semi-Lagrangian schemes
384 for Vlasov equations, *J. Comput. Phys.*, 229 (2010) 1927–1953.
- 385 [7] E. Deriaz and S. Peirani, Six-dimensional adaptive simulation of the Vlasov equations using a
386 hierarchical basis, submitted, <https://hal.archives-ouvertes.fr/hal-01419750>
- 387 [8] E. Deriaz, Personal communication.
- 388 [9] E. Fijalkow, Behaviour of phase-space holes in 2D simulations, *Journal of Plasma Physics* 61
389 (1999) 65–76.
- 390 [10] T. Fujiwara, Integration of the collisionless Boltzmann Equation for Spherical Stellar Systems,
391 *Publ. Astron. Soc. Japan* 35 (1983) 547–558.
- 392 [11] J.A.F. Hittinger and J.W. Banks, Block-structured adaptive mesh refinement algorithms for
393 Vlasov simulation, *J. Comput. Phys.* 241 (2013) 118–140.
- 394 [12] R.W Hockney and J.W Eastwood, Computer Simulation Using Particles, CRC Press, 1988.
- 395 [13] P. Koumoutsakos and A. Leonard, High resolution simulations of the flow around an impulsively
396 started cylinder, *J. Fluid Mech.* 296 (1995) 1–38.
- 397 [14] A. Magni and G.-H. Cottet, Accurate, non-oscillatory remeshing schemes for particle methods, *J.*
398 *Comput. Phys.*, 231 (2012) 152–172.

- 399 [15] A. Myers, P. Colella and B. Van Straalen, A 4th-Order Particle-in-Cell Method with Phase-Space
400 Remapping for the Vlasov-Poisson Equation, submitted, <https://arxiv.org/abs/1602.00747>
- 401 [16] D. Rossinelli, M. Bergdorf, G.H. Cottet and P. Koumoutsakos, GPU accelerated simulations of
402 bluff body flows using vortex particle methods, *J. Comput. Phys.* 229 (2010) 3316–3333.
- 403 [17] D. Rossinelli, B. Hejazialhosseini, W. van Rees, M. Gazzola, M. Bergdorf and P. Koumoutsakos,
404 MRAG–I2D: Multi-resolution adapted grids for remeshed vortex methods on multicore architec-
405 tures, *J. Comp. Phys.* 288 (2015) 1–18 .
- 406 [18] D. Rossinelli, C. Conti and P. Koumoutsakos, Mesh-particle interpolations on GPUs and multicore
407 CPUs, *Phil. Trans. R. Soc. A* 369 (2011) 2164–2175.
- 408 [19] E. Sonnendrucker, J. Roche, P. Bertrand, A. Ghizzo, The Semi-Lagrangian Method for the Nu-
409 merical Resolution of the Vlasov Equation *J. Comput. Phys.* 149 (1999) 20–220.
- 410 [20] V. Springel, The cosmological simulation code GADGET-2, *MNRAS* 364 (2005) 1105–1134.